Voltammetric sensor based on molecular imprinted polymer for lincomycin detection

Yulia A. Yarkaeva *[ID], Daria A. Dymova [ID], Marat I. Nazyrov [ID],
Liana R. Zagitova [ID], Valery N. Maistrenko [ID]

Department of Chemistry, Ufa University of Science and Technology, Ufa 450076, Russia
* Corresponding author: julijajarkaeva05@gmail.com

This paper belongs to a Regular Issue.

Abstract

For the selective detection of the antibiotic lincomycin, we developed a voltammetric sensor based on a glassy carbon electrode modified with reduced graphene oxide and polyarylenephthalide containing diphenylenethio and diphenyleneoxide fragments in the main chain of the polymer in the 1:1 ratio with lincomycin molecular imprints obtained by phase inversion. Using FTIR spectroscopy, electrochemical impedance spectroscopy, cyclic and differential-pulse voltammetry, the electrochemical and analytical characteristics of the sensor were studied. The detection of lincomycin was carried out by differential pulse voltammetry. The linear concentration range was $2.5 \cdot 10^{-7}$–$5 \cdot 10^{-4}$ M with a limit of detection of $6.8 \cdot 10^{-8}$ M. It was shown that the presence of molecular imprints increases the sensitivity of the developed sensor in comparisons with a sensor with non-imprinted polymer by a factor of 3.05.

Key findings

● MIP-sensor for the lincomycin determination based on polyarylenephthalides was obtained by phase inversion.

● The presence of molecular imprints increases the sensitivity of the MIP-sensor by a factor of 3.05.

● MIP-sensor was tested to determine lincomycin in human urine and blood plasma; RSD did not exceed 7.5%, and the recovery was 93–108%.

1. Introduction

Antibiotics are one of the most important medicines that affect human health. It is difficult to imagine modern medicine without antibiotics. However, their uncontrolled use has led to antibiotic contamination of ecosystems and food [1–4]. This has increased the already high level of resistance of many bacteria to antimicrobial drugs. The control of antibiotic content has become an urgent task for specialists in the field of environmental protection and food quality assessment, analysis of biological objects, and clinical medicine [5, 6].

To date, such analytical methods as HPLC [7], capillary electrophoresis [8], FTIR spectroscopy [9], Raman spectroscopy [10], fluorimetry [11], and microbiological methods [12] are widely used for the detection of antibiotics. Recently, electrochemical methods have been used for these

purposes, in particular, voltammetry, which makes it possible to quite simply, quickly, and with high sensitivity detect drug compounds, including antibiotics, in various matrices [13]. Various voltammetric methods, such as cyclic, differential pulse and square wave voltammetry, have been successfully applied with high selectivity and sensitivity for the analysis of drugs and the determination of antibiotics in pharmaceutical dosage forms (tablets, capsules, injections and suspensions) and biological fluids (urine samples, blood and its serum, etc.) [14–17]. When creating sensors for the detection of antibiotics, the main and most commonly employed approach to modifying electrodes is the use of molecularly imprinted polymers (MIPs) [18]. This allows solving the main problem of voltammetry, i.e., insufficient selectivity of detections. Such an approach is analogous to antibody-antigen or enzyme-substrate interactions (key-lock interactions) in biological systems. It is based on

the polymerization of a monomer in the presence of a template molecule, with the resulting polymer containing specific cavities of the analyte after its removal from the polymer [19, 20]. Compared to antibodies, MIPs are cheaper, more stable, and withstand a wider range of pH and temperature [21]. The development of MIP for modifying electrodes in voltammetry includes several key steps: polymerization or polymer deposition; removal of the template (usually by a solvent or electrochemical method); instrumental measurements. MIPs can be obtained using various methods of monomer polymerization in the presence of a template molecule (chemical, electrochemical, photopolymerization). In addition to polymerization, the phase inversion method can be used to create MIP-sensors [22]. The method consists in the use of ready-made polymers that are deposited on the surface of the working electrode from a solution in the presence of the analyte. Its main advantage is the simplicity and faster manufacturing of the MIP-sensor. To dissolve the two components, a solvent is chosen that is compatible with both the main polymer and the template. Their mixing makes it possible to form a "guest-host" complex in solution. MIP can be obtained in two ways: 1) wet phase inversion (WPI) – by adding another solvent, which causes the precipitation of the polymer associated with the template; 2) dry phase inversion (DPI) – the MIP-membrane is obtained by evaporating the solvent from the polymer during the heating process [23]. The DPI method is simpler and more convenient to manufacture, since, unlike WPI, it does not require the selection of a second solvent. WPI is also complicated by the fact that the template may not be deposited in the polymer composition or may be deposited in a very small amount, which leads to a low specificity of the resulting MIP. DPI is usually carried out with heat. Therefore, in this case, polyarylenephthalides (PAP) [24–26], which are electrically conductive in thin layers and chemically resistant to heat and aggressive media, are of considerable interest and can be used. PAPs were previously studied and applied in the manufacture of sensors for the creation of composite materials [15].

The selectivity and sensitivity of MIP-sensors are their main and most important characteristics. However, the deposition of a polymer on the electrode surface often leads to a decrease in currents due to an increase in resistance. Therefore, components that increase electrical conductivity must be added to the sensor layer. Recently, nanomaterials have been used for these purposes, such as Au and Pt nanoparticles, single-walled and multi-walled carbon nanotubes, reduced graphene oxide (rGO) [13, 17, 27], etc. At the same time, rGO is also used as a convenient matrix for immobilizing various components when creating efficient sensor platforms based on composite materials and increasing the sensitivity and selectivity of voltammetric sensors due to its unique properties, such as high electrical conductivity, large specific surface area, mechanical strength, etc.

Lincomycin hydrochloride (Lin) (Figure 1a), derived from Streptomyces lincolnensis, is a well-established antibiotic. It is active against most common Gram-positive bacteria, inhibits cell growth and microbial protein synthesis, and is used to treat many infectious diseases [28] (staphylococcal, streptococcal, bacteroid infections, pneumonia, anthrax, furunculosis, carbuncles, impetigo, burns and wounds).

In this work, to determine Lin, a voltammetric sensor based on a glassy carbon electrode (GCE) modified with rGO and PAP containing diphenylenethio- and diphenyleneoxide fragments in the main chain of the polymer in 1:1 ratios (Figure 1b) was developed. The characteristics of the sensor were studied using FTIR spectroscopy, electrochemical impedance spectroscopy (EIS), and cyclic voltammetry (CV). Lin was determined by differential pulse voltammetry (DPV). The analytical characteristics of the developed sensors, such as sensitivity, selectivity, linear range of concentrations and limit of detection (LOD), were studied.

2. Experimental

2.1. Materials and reagents

Lin (≥99.5%), $K_3Fe(CN)_6$ (≥99.0%) and $K_4Fe(CN)_6$ (≥99.0%), GO powder (15–20 sheets, 4–10% edge oxidation) were purchased from Sigma-Aldrich (USA). Samples of the PAP polymer (spectroscopically pure) were provided by the Laboratory for the Synthesis of Functional Polymers, Ural Federal Research Center, Russian Academy of Sciences (Ufa, Russia) [24–26]. The supporting electrolyte for Lin was a phosphate buffer solution (PBS, KH_2PO_4 + Na_2HPO_4, 0.1 M, pH 6.9). A 0.5 mM Lin solution was prepared by dissolving an accurate weighed portion of the reagent in 25 mL of PBS. Solutions of lower concentrations were prepared by serial dilution. Urine samples were obtained with the written consent of the donor, blood plasma was purchased from the Ufa Republican Blood Transfusion Station. Urine and blood plasma samples, 2.5 ml in volume, were centrifuged for 10 min and diluted 10 times with PBS pH 6.9. Known amounts of Lin were added to the resulting solutions to obtain solutions with concentrations of 0.35 and 0.04 mM. All solutions were prepared using ultrapure deionized water with a specific electrical conductivity of 0.1 μS cm⁻¹.
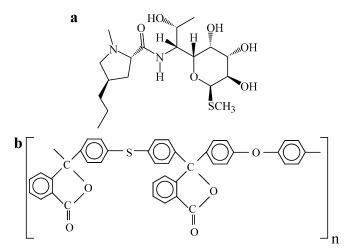

Figure 1 Structure of Lin (a) and PAP polymer (b).

All electrochemical measurements were performed on Autolab PGSTAT 204 potentiostat-galvanostat with an FRA32M impedance module (Metrohm Autolab Ins., Netherlands) with NOVA software. A standard three-electrode cell consisted of a modified GCE (Metrohm Autolab Ins., Netherlands) with a diameter of 3 mm as a working electrode, a platinum plate as an auxiliary electrode, and a silver chloride electrode with a 3.5 M KCl solution as a reference electrode. The pH of solutions was measured using a Seven Compact pH/Ion S220 pH meter (Mettler-Toledo AG, Switzerland). The solutions were stirred using an MR Hei-Tec magnetic stirrer (Heidolph, Germany). FTIR spectra of GO and rGO were recorded in the range 450–3500 cm^{-1} on an FTIR-8400S spectrometer (Shimadzu, Japan) at room temperature (resolution 8 cm^{-1}, number of scans 30) with IR solution software.

2.2. Modification of the electrode surface

To modify the GCE, 4 mg of GO was added to 1 ml of an aqueous ethanol solution (at a ratio of $C_2H_5OH:H_2O$ 1:1), after which it was sonicated for 1 hour. GO dispersed in an aqueous ethanol solution was applied dropwise onto a carefully polished GCE surface and dried under an IR lamp. The reduction of GO was carried out in a potentiostatic mode at a potential of $E = -0.8$ V for 3 minutes in a phosphate buffer solution. The conditions of GO reduction were chosen experimentally according to the values of Lin oxidation currents and RSD. To prepare mixtures of polymers with a template, 10 mg of the polymer and 5 mg of Lin were dissolved in 10 ml of N,N-Dimethylformamide (DMF). The polymer:template ratio was experimentally found to be optimal according to the Ip and relative standard deviation (RSD) values. The resulting polymer solutions with the template were applied to the GCE surface modified with rGO, followed by removal of the template in 1 M NaOH solution for 120 s with stirring. A sensor with a non-imprinted polymer (NIP) was obtained by a similar procedure, but without the addition of a template.

2.3. Experimental techniques

Differential pulse voltammograms (DPV) were recorded in the potential range from 0 to 1.2 V with a scan rate of 20 mV s^{-1}. Electrochemical impedance spectra were recorded in the frequency range from 500 kHz to 0.1 Hz with an amplitude of 10 mV. Cyclic voltammograms were recorded in the potential range from 0 to 1.3 V with a scan rate of 0.1 mV s^{-1}. Before recording the DPV, the sensor was kept in the analyte solution for 80 s to incubate Lin. All measurements were carried out at a temperature of 25±0.1 °C.

3. Results and Discussion

3.1. FTIR and EIS results

As a rule, rGO is used in electrochemical sensors to remove carboxyl and carbonyl groups and increase the electrical conductivity of the material. The FTIR spectrum (Figure 2)

of GO shows characteristic bands at 1025, 1223, 1414, 1715, and 3419 cm^{-1}, which can be attributed to the stretching vibrations C–O, C–O–C, C–OH, C=O and –OH, while on rGO these characteristic bands sharply decrease or disappear, confirming that GO is reduced to rGO. The stretching vibrations at 1640 cm^{-1}, observed both in GO and rGO, correspond to the C=C bonds present in the graphene sheet. The obtained FTIR spectra agree with the literature data [29]. The characteristic bands in the Lin spectrum are those at 1657 and 1567 cm^{-1}, corresponding to the C=O stretching vibrations and N–H bending vibrations of the amide group, respectively. Stretching of S–CH$_3$ is observed at 1107 cm^{-1}, N–H – at 1041 cm^{-1}, C–O–C (ether bond) – at 1263 cm^{-1}, C–H (aliphatic) – at 2955 cm^{-1}. A wide band of O–H stretching vibrations with a complex contour is observed at 3528–3289 cm^{-1}, which, moreover, overlaps the N–H stretching vibrations. The characteristic bands in the PAP spectrum are 1770 and 1078 cm^{-1}, corresponding to the C=O and C–O–C bonds of the phthalide group, 757 cm^{-1} corresponds to the Ar–S–Ar bond, 1244 cm^{-1} – to the Ar–O–Ar bonds. The characteristic bands of Lin appear in the spectrum of the PAP-Lin complex. And the band at 1770 cm^{-1}, corresponding to C=O, shifts to 1758 cm^{-1}, which may be due to the participation of this group in the formation of a hydrogen bond.

EIS with $[Fe(CN)_6]^{3-/4-}$ showed that each modification stage has a different effect on the currents of the $[Fe(CN)_6]^{3-/4-}$ redox pair. The lowest resistance to electron transfer R_{et} was observed on GCE/rGO (Figure 3a, curve 3), while on unreduced GO (curve 2) the resistance is higher. When a PAP polymer film is deposited on GCE/rGO, the resistance increases (curve 4), but it does not significantly exceed the resistance on bare GCE, which is due to the electrical conductivity of the PAP. After Lin is washed out of the polymer, R_{et} decreases (curve 5) and the electron transfer rate increases due to the formation of pores in polymers through which $[Fe(CN)_6]^{3-/4-}$ ions penetrate.
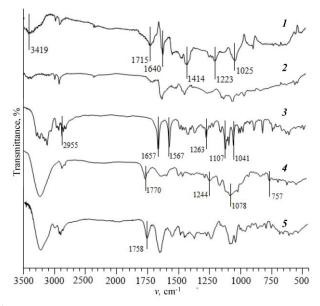

Figure 2 FTIR spectra of GO (1), rGO (2), Lin (3), PAP (4), PAP-Lin (5).
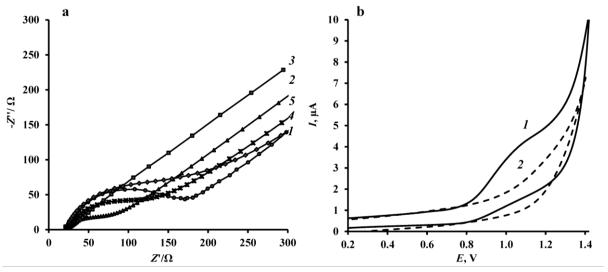
Figure 3 Nyquist diagrams of GCE (1), GCE/GO (2), GCE/rGO (3), GCE/rGO/PAP (4), GCE/rGO/miPAP (5) in 5 mM [Fe (CN)$_6$]$^{3-/4-}$ (1:1, 0.1 M KCl, 0.1 V s^{-1}) (a); CV of the supporting electrolyte on GCE/rGO/miPAP before (1) and after (2) washing out of Lin from the polymer film in the supporting electrolyte (pH 6.9, 0.1 V s^{-1}) (b).

Also, Figure 3b shows that the CVs obtained in the supporting electrolyte solution before and after Lin was washed out from the polymer film differ: curve 1 shows a small peak of Lin oxidation due to the presence of Lin in the polymer film, which disappears after washing out in a 1 M NaOH solution with stirring for 120 s (Figure 3b, curve 2), confirming the effectiveness of the chosen technique.

3.2. Quantum-chemical modeling of the interaction of Lin with the PAP polymer

Based on the structure of Lin, hydroxyl groups in the galactopyranose fragment can be identified as possible centers of interaction, which suggests a tendency to form hydrogen bonds. The lactone fragments of the phthalide blocks of the polymer contain oxygen atoms, which can act as hydrogen bond acceptors. To calculate possible interactions, the following simplification was introduced: two blocks consisting of two units were used as a polymer. After the initial optimization of the structures by the AM1 semi-empirical method, possible complexes were calculated by the CHARMM method [30] in the HyperChem program (Figure 4). The possibility of hydrogen bonding (2.017 Å, 2.668 Å and 2.713 Å) and the formation of cavities in the polymer for the antibiotic molecule was confirmed.

3.3. Lin detection

Lin electrooxidation is a one-electron one-proton process with the formation of a dimerized product [6]. Figure 5 shows the DPV of a Lin solution on bare GCE, GCE/rGO, on GCE modified with PAP, and on GCE modified with molecularly imprinted PAP (miPAP). The deposition of GO on the surface of the GCE with subsequent electrochemical reduction leads to an increase in the sensitivity of the sensor to Lin, as well as to a shift in the oxidation potential of Lin to the cathode region, which, apparently, is due to the facilitation of the process of its oxidation on GO. The obtained DPVs of the Lin solution on GCE/rGO/miPAP are consistent with the previously obtained EIS data.

The linear range of the dependence of Lin oxidation current on its content in the solution on GCE/rGO/miPAP remains in the concentration range from 2.5·10^{-7} to 5·10^{-4} M, with a detection limit of 6.8·10^{-8} M (Figure 6).

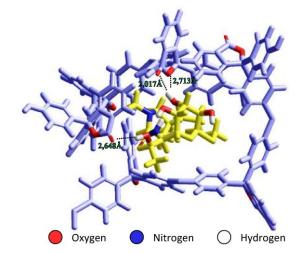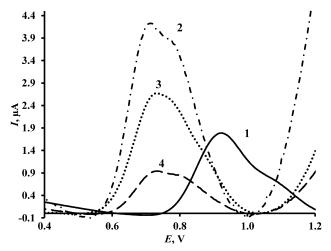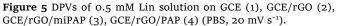**Figure 4** Possible interactions between PAP-polymer (blue) and Lin (yellow) optimized by the quantum chemical modeling.

Figure 5 DPVs of 0.5 mM Lin solution on GCE (1), GCE/rGO (2), GCE/rGO/miPAP (3), GCE/rGO/PAP (4) (PBS, 20 mV s^{-1}).

In addition, Figure 6b shows the calibration curves obtained at each stage of the GCE modification. The corresponding equations are as follows:

$$y = (2.99\pm0.16)x + (0.27\pm0.02), R^2 = 0.9966, \quad (1)$$

$$y = (6.21x\pm0.26) + (0.88\pm0.04), R^2 = 0.9914, \quad (2)$$

$$y = (1.63\pm0.13)x + (0.12\pm0.03), R^2 = 0.9971, \quad (3)$$

$$y = (4.97\pm0.21)x + (0.37\pm0.02), R^2 = 0.9975. \quad (4)$$

It can be seen that in all curves there is a linear dependence of the peak current on the Lin concentration. The selectivity coefficients S on the GCE are lower than those on the final sensor. It should be noted that the sensitivity on GCE/rGO is higher than that on GCE/rGO/miPAP, which is associated with an increase in resistance when using the PAP-polymer, being consistent with the EIS data. However, the resulting S and LOD on GCE/rGO/miPAP is sufficient to detect Lin in real samples [31–33]. The linear dependences on GCE/rGO/PAP and GCE/rGO/miPAP show that the presence of molecular imprints increases the sensitivity of GCE/rGO/miPAP by a factor of 3.05 (S_{MIP}/S_{NIP}). These results illustrate the high sensitivity and selectivity of the GCE/rGO/miPAP sensor.

The obtained results show that the developed sensor for Lin detecting is comparable to the electrochemical sensors described in the literature, are not inferior to them in their characteristics, and sometimes even surpass them (Table 1). This confirm the good sensitivity of GCE/rGO/miPAP in Lin detection. It should be noted that the sensor fabrication procedure has a simple strategy and lower number of steps for creating MIP due to the use of the phase inversion method; as a result, this approach is more express. Other methods listed in Table 1 such as elec-

trochemiluminescence, surface plasmon resonance, Raman spectroscopy, colorimetric, photoelectrochemical methods can detect Lin with a lower LOD. However, according to [31–33], the concentration of Lin and its analogues in biological fluids is 0.25–16 µg mL⁻¹ (i.e. $1.2\cdot10^{-6}$–$3.9\cdot10^{-5}$ M). Thus, the LOD of the developed sensor is sufficient to detect Lin.

To estimate the correctness of the detection of Lin, the "spike-recovery" test was used (Table 2). The sensor made it possible to detect the Lin concentration with high accuracy over the entire linear range; the RSD did not exceed 3.6%, which indicates good reproducibility of the detection, and the values of the relative measurement error not exceeding 3% indicate the accuracy of the results. To assess the analytical capabilities of the proposed sensor, it was used to detect Lin in human urine and blood plasma. The RSD did not exceed 7.5%, and the recovery was 93–108%. Statistical evaluation of the measurement results by the "spike-recovery" test indicates the absence of a significant systematic error.

The repeatability and stability tests of the GCE/rGO/miPAP were carried out for $5\cdot10^{-4}$ mM Lin. After 10 successive assays, the response signal of the GCE/rGO/miPAP still remained up to 97.1% of its initial values with RSD 3.9%. After 10 days of storage at room temperature, the current responses of the GCE/rGO/miPAP remained up to 95.3% of its initial value with RSD 4.1%.

4. Limitations

When recording the DPV, the capacitive currents on the GCE and the GCE modified with rGO differ significantly. In this regard, it is necessary to carry out the baseline correction, as well as the curve smoothing based on the Savitzky-Golay algorithm.
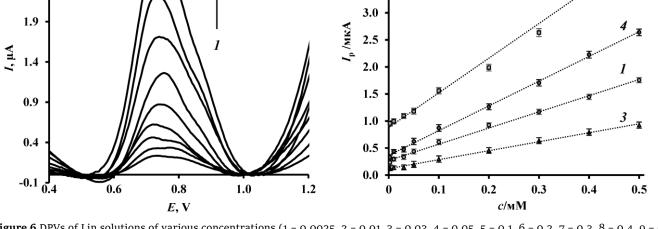

Figure 6 DPVs of Lin solutions of various concentrations (1 – 0.0025, 2 – 0.01, 3 – 0.03, 4 – 0.05, 5 – 0.1, 6 – 0.2, 7 – 0.3, 8 – 0.4, 9 – 0.5 mM) on GCE/rGO/miPAP (a); calibration curves of GCE (1), GCE/rGO (2), GCE/rGO/PAP (3) and GCE/rGO/miPAP (4) sensors (PBS, 20 mV s⁻¹, $n = 5$, $P = 0.95$) (b).

Table 1 Figures of merit of proposed sensor GCE/rGO/miPAP in comparison with the reported electrochemical sensors and other methods used for the Lin detection.

Sensing element	Technique	Linear range, M	LOD, M	References
Electrochemical sensors				
GCE/rGO/miPAP	DPV	$2.5 \cdot 10^{-7} – 5 \cdot 10^{-4}$	$6.8 \cdot 10^{-8}$	This work
MWNTs-DHP/GCE	CV	$4.5 \cdot 10^{-7} – 1.5 \cdot 10^{-4}$	$2.0 \cdot 10^{-7}$	[5]
Au	DPV	$8.0 \cdot 10^{-6} – 1.0 \cdot 10^{-4}$	$1.7 \cdot 10^{-7}$	[6]
BDD thin film electrodes	CV	$5.0 \cdot 10^{-7} – 1.3 \cdot 10^{-4}$	$2.0 \cdot 10^{-8}$	[34]
DME in KH_2PO_4-Na_2HPO_4-$K_2S_2O_8$ solution	CV	$8.5 \cdot 10^{-8} – 9.0 \cdot 10^{-5}$	$4.0 \cdot 10^{-8}$	[35]
Au-PtNPs/nanoPAN/CS/GCE	CV	$7.4 \cdot 10^{-6} – 2.5 \cdot 10^{-4}$	$2.5 \cdot 10^{-6}$	[36]
Other methods				
MIP-Au-GO/GCE	ECL	$5.0 \cdot 10^{-12} – 1.0 \cdot 10^{-9}$	$1.6 \cdot 10^{-13}$	[37]
SnO_2/chitosan/g-C_3N_4/GCE	ECL	$2.5 \cdot 10^{-10} – 2.5 \cdot 10^{-7}$	$6.9 \cdot 10^{-11}$	[38]
N-doped Ti_3C_2 QDs/BiOBr	PEC	$1.0 \cdot 10^{-14} – 1.0 \cdot 10^{-8}$	$3.6 \cdot 10^{-15}$	[39]
PFCs-TiO_2/NG/ITO- ZnPc/MoS_2/ITO	PEC	$1.0 \cdot 10^{-11} – 1.0 \cdot 10^{-5}$	$3.3 \cdot 10^{-12}$	[40]
$HAuCl_4$/NaOH solution	Colorimetry	$1.0 \cdot 10^{-6} – 2.5 \cdot 10^{-5}$	$9.7 \cdot 10^{-7}$	[41]
Au-Pt NR-apt/cDNA/PTP/Eu MOF/GCE	ECL-SPR	$2.5 \cdot 10^{-10} – 2.5 \cdot 10^{-4}$	$6.4 \cdot 10^{-11}$	[42]
mAb-AuNPs-DTNB	SERS	$2.5 \cdot 10^{-13} – 2.5 \cdot 10^{-9}$	$7.1 \cdot 10^{-13}$	[43]
CdS QDs/C-g-C_3N_4	ECL	$1.2 \cdot 10^{-11} – 2.5 \cdot 10^{-4}$	$4.9 \cdot 10^{-11}$	[44]

MWNTs – multi-wall carbon nanotubes; DHP – dihexadecylphosphate; BDD – boron-doped diamond; DME – dropping mercury electrode; Au-PtNPs – Au-Pt alloy nanoparticles; nanoPAN – polyaniline nanotube; CS – chitosan; g-C_3N_4 – graphene-like carbon nitride; QDs – quantum dots; TiO_2/NG – nitrogen-doped graphene-loaded TiO_2 nanoparticles; PFC – dualphotoelectrode photofuel cell; ZnPc/MoS_2 – zinc phthalocyanine nanoparticles sensitized MoS_2; ITO – indium tin oxide; NR – nanorod; apt/cDNA – bridge of aptamer and complementary DNA; PTP – PTCA (perylene tetracarboxylic dianhydride) – PANI (polyanilin); Eu MOF – europium metal–organic framework; AuNPs – gold nanoparticles; DTNB – 5,5′-dithiobis (2-nitrobenzoic acid); mAb – monoclonal antibody; C-g-C_3N_4 – carboxylated g-C_3N_4; ECL – electrochemiluminescence; PEC – photoelectrochemical; SPR – surface plasmon resonance; SERS – surface-enhanced Raman spectroscopy.

Table 2 Lin determination using DPV on the GCE/rGO/miPAP (PBS, 20 mV s^{-1}, $n = 5$, $P = 0.95$).

	Spiked, µM	Found, µM	RSD, %	Recovery, %
Lin solution	350	353±9	1.9	101
	40	41±6	2.7	103
Lin in urine	350	346±15	6.6	99
	40	43±5	5.2	108
Lin in blood plasma	350	343±11	7.5	98
	40	37±6	5.3	93

5. Conclusions

Thus, to detect the antibiotic Lin, we developed the sensor based on GCE modified with rGO and molecularly imprinted PAP obtained by phase inversion by solvent evaporation. It should be noted that when the phase inversion method is used to obtain the MIP, the sensor manufacturing process is greatly simplified. It was shown that the developed sensor has a high selectivity for the detected antibiotic, and the presence of specific binding sites in the polymer film makes it possible to detect Lin with a sensitivity that is 3.05 times higher than that of a similar sensor without molecular imprints. The resulting sensor was successfully used to determine Lin in biological fluids.

● Supplementary materials

No supplementary materials are available.

● Author contributions

Conceptualization: V.N.M., Y.A.Y.
Data curation: Y.A.Y.
Formal Analysis: M.I.N., Y.A.Y., L.R.Z.
Funding acquisition: Y.A.Y., D.A.D.
Investigation: D.A.D., M.I.N.
Methodology: V.N.M., Y.A.Y.
Project administration: Y.A.Y.
Resources: Y.A.Y.
Supervision: V.N.M.
Validation: D.A.D., Y.A.Y.
Visualization: D.A.D., M.I.N., Y.A.Y., L.R.Z.
Writing – original draft: Y.A.Y., M.I.N.
Writing – review & editing: V.N.M.

● Conflict of interest

The authors declare no conflict of interest.

● Additional information

Author IDs:

Yulia A. Yarkaeva, Scopus ID 56872864300;
Daria A. Dymova, Scopus ID 57899452900;
Marat I. Nazyrov, Scopus ID 57330245700;
Liana R. Zagitova, Scopus ID 57201803011;
Valery N. Maistrenko, Scopus ID 6603789725.

Website:

Ufa University of Science and Technology, https://uust.ru/page-contacts.

References

1. Pham THY, Mai TT, Nguyen HA, Chu TTH, Vu TTH, Le QH. Voltammetric determination of amoxicillin using a reduced graphite oxide nanosheet electrode. J Anal Methods Chem. 2021;2021:8823452. doi:10.1155/2021/8823452

2. Valenga MGP, Felsner ML, de Matos CF, de Castro EG, Galli A. Development and validation of voltammetric method for determination of amoxicillin in river water. Anal Chim Acta. 2020;1138:79–88. doi:10.1016/j.aca.2020.09.020

3. Li H, Xu B, Wang D, Zhou Y, Zhang H, Xia W, Xu S, Li Y. Immunosensor for trace penicillin G detection in milk based on supported bilayer lipid membrane modified with gold nanoparticles. J Biotechnol. 2015;203:97–103. doi:10.1016/j.jbiotec.2015.03.013

4. Bougrini M, Florea A, Cristea C, Sandulescu R, Vocanson F, Errachid A, Bouchikhi B, Bari NE. Development of a novel sensitive molecularly imprinted polymer sensor based on electropolymerization of a microporous-metal-organic framework for tetracycline detection in honey. Food Control. 2016;59:424–429. doi:10.1016/j.foodcont.2015.06.002

5. Wu Y, Ye S, Hu S. Electrochemical study of lincomycin on a multi-wall carbon nanotubes modified glassy carbon electrode and its determination in tablets. J Pharm Biomed Anal. 2006;41:820–824. doi:10.1016/j.jpba.2006.01.037

6. Abbar JC, Meti MD, Nandibewoor ST. Anodic Voltammetric behavior of lincomycin and its electroanalytical determination in pharmaceutical dosage form and urine at gold electrode. Z Phys Chem. 2017;231(5):957–970. doi:10.1515/zpch-2015-0745

7. Prado TM, Foguel MV, Gonçalves LM, Sotomayor MPT. β-Lactamase-based biosensor for the electrochemical determination of benzylpenicillin in milk. Sens Actuators B Chem. 2015;210:254–258. doi:10.1016/j.snb.2014.12.108

8. Samanidou V, Nisyriou S Multi-residue methods for confirmatory determination of antibiotics in milk. J Sep Sci. 2008;31(11):2068–2090. doi:10.1002/jssc.200700647

9. Mohsenzadeh MS, Mohammadinejad A, Mohajeri SA. Simple and selective analysis of different antibiotics in milk using molecularly imprinted polymers: a review. Food AdditContam Part A. 2018;35(10):1959–1974. doi:10.1080/19440049.2018.1508889

10. Bitas D, Samanidou V. Molecularly imprinted polymers as extracting media for the chromatographic determination of antibiotics in milk. Molec. 2018;23(2):316. doi:10.3390/molecules23020316

11. Kennedy DG, McCracken RJ, Cannavan A, Hewitt SA. Use of liquid chromatography–mass spectrometry in the analysis of residues of antibiotics in meat and milk. J Chromatogr A. 1998;812(1–2):77–98. doi:10.1016/S0021-9673(98)00048-X

12. Cañada-Cañada F, Muñoz de la Peña A, Espinosa-Mansilla A. Analysis of antibiotics in fish samples. Anal Bioanal Chem. 2009;395(4):987–1008. doi:10.1007/s00216-009-2872-z

13. Yarkaeva Y, Maistrenko V, Dymova D, Zagitova L, Nazyrov M. Polyaniline and poly(2-methoxyaniline) based molecular imprinted polymer sensors for amoxicillin voltammetric determination. Electrochim Acta. 2022;433:141222. doi:10.1016/j.electacta.2022.141222

14. Zagitova L, Maistrenko V, Yarkaeva Y, Zagitov V, Zilberg R, Kovyazin P, Parfenova L. Novel chiral voltammetric sensor for tryptophan enantiomers based on 3-neomenthylindene as recognition element. J Electroanal Chem. 2021;880:114939. doi:10.1016/j.jelechem.2020.114939

15. Yarkaeva Y, Maistrenko V, Zagitova L, Nazyrov M, Berestova T. Voltammetric sensor system based on Cu(II) and Zn(II) amino acid complexes for recognition and determination of atenolol enantiomers. J Electroanal Chem. 2021;903:115839. doi:10.1016/j.jelechem.2021.115839

16. Yarkaeva Y, Islamuratova E, Zagitova L, Gus'kov V, Zil'berg R, Maistrenko V. A Sensor for the recognition and determination of tryptophan enantiomers based on carbon-paste electrode modified by enantiomorphic crystals of bromotriphenylmethane. J Anal Chem. 2021;76(11):1345–1354. doi:10.1134/S1061934821110162

17. Zagitova L, Yarkaeva Y, Zagitov V, Nazyrov M, Gainanova S, Maistrenko V. Voltammetric chiral recognition of naproxen enantiomers by N-tosylproline functionalized chitosan and reduced graphene oxide based sensor. J Electroanal Chem. 2022;992:116774. doi:10.1016/j.jelechem.2022.116744

18. Benachio I, Lobato A, Goncalves LM. Employing molecularly imprinted polymers in the development of electroanalytical methodologies for antibiotic determination. J Mol Recognit. 2021;34:2878. doi:10.1002/jmr.2878

19. Wulff G. Fourty years of molecular imprinting in synthetic polymers: origin, features and perspectives. Microchim Acta. 2013;180(15–16):1359–1370. doi:10.1007/s00604-013-0992-9

20. Baeza-Fonte AN, Garcés-Lobo I, Luaces-Alberto MD, Gonçalves LM, Sotomayor M, Valdés-González AC. Determination of cephalosporins by UHPLC-DAD using molecularly imprinted polymers. J Chromatogr Sci. 2018;56(2):187–197. doi:10.1093/chromsci/bmx099

21. Alenazi NA, Manthorpe JM, Lai EPC. Selectivity enhancement in molecularly imprinted polymers for binding of bisphenol A. Sensors. 2016;16(10):1697. doi:10.3390/s16101697

22. Gavrila AM, Stoica EB, Iordache TV, Sârbu A. Modern and dedicated methods for producing molecularly imprinted polymer layers in sensing applications. Appl Sci. 2022;12:3080. doi:10.3390/app12063080

23. BelBruno J. Molecularly imprinted polymers. Chem Rev. 2019;119:94–119. doi:10.1021/acs.chemrev.8b00171

24. Kraikin V, Fatykhov A, Gileva N, Kravchenko A, Salazkin S. NMR study of dyadic and triadic splitting in copoly(arylene)phthalides based on diphenyl oxide and diphenyl sulfide. Magn Reson Chem. 2020;59(1):61–73. doi:10.1002/mrc.5079

25. Salazkin S, Shaposhnikova V, Machulenko L, Gileva N, Kraikin V, Lachinov A. Synthesis of polyarylenephthalides prospective as smart polymers. Polym Sci Ser A. 2008;50(3):243–259. doi:10.1134/S0965545X08030024

26. Gileva N, Kraikin V, Sedova E, Lobov M, Kuznetsov S, Salazkin S. Control over the composition and microstructure of copoly(arylene phthalides). Russ J Appl Chem. 2005;78(10):1683–1686.

27. Salikhov R, Zilberg R, Mullagaliev I, Salikhov T, Teres Y. Nanocomposite thin film structures based on polyarylenephthalide with SWCNT and graphene oxide fillers. Mendeleev Commun. 2022;32:520–522. doi:10.1016/j.mencom.2022.07.029

28. Hardman JG, Limbird LE, Gilman AG. Goodman & Gilman's the pharmacological basis of therapeutics. 10th Edition. New York: McGraw-Hill; 2001. 256 p.

29. Luo H, Li H, Ge Q, Cong H, Tao Z, Liu M. An electrochemical sensor for enantio-recognition of tyrosine based on a chiral macrocycle functionalized rGO. Microchem J. 2021;164:105949. doi:10.1016/j.microc.2021.105949

30. Wu YY, Zhao FQ, Ju XH, A comparison of the accuracy of semi-empirical PM3, PDDG and PM6 methods in predicting heats of formation for organic compounds. J Mex Chem Soc. 2014;58:223–229. doi:10.29356/jmcs.v58i2.182

31. Girondi NG, Barreto F, Pigatto MC, Dalla Costa T. Sensitive analytical method to quantify clindamycin in plasma and microdialysate samples: Application in a preclinical pharmacokinetic study. J Pharm Biomed Anal. 2018;153:57–62. doi:10.1016/j.jpba.2018.02.005

32. Hu Y, Zhu Q, Wang Y, Liao C, Jiang G. A short review of human exposure to antibiotics based on urinary biomonitoring. Sci Total Environ. 2022;830:154775. doi:10.1016/j.scitotenv.2022.154775

33. Gouri SS, Venkatachalam D, Dumka VK. Pharmacokinetics of lincomycin following single intravenous administration in buffalo calves. Trop Anim Health Prod. 2014;46:1099–1102. doi:10.1007/s11250-014-0595-4

34. Boonsong K, Chuanuwatanakul S, Wangfuengkanagul N, Chailapakul O. Electroanalysis of lincomycin using boron-doped diamond thin film electrode applied to flow injection system. Sensors Actuators B. 2005;108:627–632. doi:10.1016/j.snb.2004.12.087

35. Li N, Song J, Wei Guo, Xu M. Study and application of parallel catalytic hydrogen wave of lincomycin in the presence of persulfate. Microchem J. 2004;77:23–28. doi:10.1016/j.microc.2003.10.001

36. Wang X, Yang T, Jiao K. Electrochemical study of lincomycin on Au-PtNPs/nanoPAN/ Chitosan nanocomposite membrane and its determination in injections. Chem Res Chin Univ. 2010;26(3):371–375.

37. Li S, Liu C, Yin G, Zhang Q, Luo J, Wu N. Aptamer-molecularly imprinted sensor base on electrogenerated chemiluminescence energy transfer for detection of lincomycin. Biosensors Bioelectron. 2017;91:687–691. doi:10.1016/j.bios.2017.01.038

38. Liu X-P, Huang B, Mao C-J, Chen J-S, Jin B-K. Electrochemiluminescence aptasensor for lincomycin antigen detection by using a SnO_2/chitosan/g-C_3N_4 nanocomposite. Talanta. 2021;233:122546. doi:10.1016/j.talanta.2021.122546

39. Wei M, Du X, Zhang Y, Shan X, Wang W, Chen Y, Jiang D, Xu F, Shiigi H, Chen Z. Ultrasensitive self-driven photoelectrochemical aptasensor for lincomycin detection based on oxygen vacancy-tunable BiOBr nanosheet coupled with dual-function of N-doped Ti_3C_2 quantum dots. Biosensors Bioelectron. 2022;12:100266. doi:10.1016/j.biosx.2022.100266

40. Wen Z, Ding L, Zhang M, You F, Yuan R, Wei J, Qian J, Wang K. A membrane/mediator-free high-power density dual-photoelectrode PFC aptasensor for lincomycin detection in milk and chicken. Anal Chim Acta. 2023;1245:340880. doi:10.1016/j.aca.2023.340880

41. Leng Y, Hu F, Ma C, Du C, Ma L, Xu J, Lin Q, Sang Z, Lu Z. Simple, rapid, sensitive, selective and label-free lincomycin detection by using $HAuCl_4$ and NaOH. RSC Adv. 2019;9:28248–28252. doi:10.1039/C9RA04095A

42. Li J, Luo M, Jin C, Zhang P, Yang H, Cai R, Tan W. Plasmon-Enhanced Electrochemiluminescence of PTP-Decorated Eu MOF-Based Pt-tipped au bimetallic nanorods for the lincomycin Assay. Eur Food Res Technol. 2022;248:2157–2165. doi:10.1021/acsami.1c21528

43. Shi Q, Tao C, Kong D. Multiplex SERS-based lateral flow assay for one-step simultaneous detection of neomycin and lincomycin in milk. Eur Food Res Technol. 2022;248:2157–2165. doi:10.1007/s00217-022-04038-3

44. Fan Y, Liu Z, Wang J, Cui C, Hu L. An "off–on" electrochemiluminescence aptasensor for determination of lincomycin based on CdS QDs/carboxylated g-C_3N_4. Microchim Acta. 2023;190(1):11. doi:10.1007/s00604-022-05587-w